Powder Technology 486 (2027) 123244

Contents lists available at ScienceDirect

Powder Technology

journal homepage: www.journals.elsevier.com/powder-technology

Particle tracking in a circulating fluidized bed via borescopic high-speed imaging

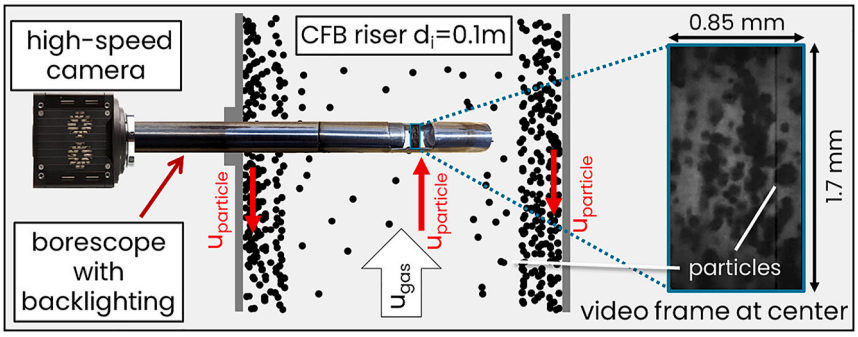
Lennard Lindmüller [a,*], Stefan Heinrich [a], Benjamin Rahimian [b], Jörg Theuerkauf [c], Yuan Yao [d], Yi Fan [d]

[a] Hamburg University of Technology, Institute of Solids Process Engineering and Particle Technology, Hamburg, Germany
[b] University College London, Dept. of Chemical Engineering, London, UK
[c] Applied Engineering and Process Technology, Core R&D, The Dow Chemical Company, Midland, MI, USA
[d] Applied Engineering and Process Technology, Core R&D, The Dow Chemical Company, Lake Jackson, TX, USA

HIGHLIGHTS

- Borescopic high speed imaging for particle tracking in circulating fluidized bed.
- Evaluation of single particle velocity trends via particle tracking velocimetry.
- Radial velocity trends correspond to solids concentrations from capacitance probes.
- Overall trends were cross-validated with pressure and solids flux measurement.

GRAPHICAL ABSTRACT



ARTICLE INFO

Keywords:
Fast fluidization
Circulating fluidized bed
Borescopic high-speed imaging
Particle tracking velocimetry

ABSTRACT

This study investigates the hydrodynamic behavior of particles in the fast fluidization regime in a pilot-scale circulating fluidized bed riser ($d_{i,riser}$ = 0.1 m, h = 8 m). Measurements were carried out using fluid catalytic cracking catalyst (FCC) with a Sauter mean diameter of 61.5 μm at superficial gas velocities from 2 to 5 m/s and solids fluxes from 3.1 to 19.3 kg/(m^{2}s) in the fully developed flow region. A borescopic high-speed camera system enabled radial measurements of individual particle trajectories via particle tracking velocimetry (PTV). Radial solids concentration profiles were evaluated using capacitance probes. A typical core-annular flow was observed in the riser, with low solids concentrations in the center and higher concentrations in the wall region. Local solids fluxes derived from solids concentration and velocity data were consistent with directly measured solids fluxes. Overall, this work provides a comprehensive experimental dataset on particle hydrodynamics in CFB systems, serving as reference data for computational fluid dynamics/discrete element method (CFD-DEM) model validation.

* Corresponding author.
E-mail address: lennard.lindmueller@tuhh.de (L. Lindmüller).

https://doi.org/10.1016/j.powtec.2026.123244
Received 13 March 2026; Received in revised form 27 August 2026; Accepted 15 September 2026
Available online 17 September 2026
0032-5910/© 2026 The Authors. Published by Elsevier B.V. This is an open access article under the CC BY license (http://creativecommons.org/licenses/by/4.0/).
Open access funding enabled and organized by Projekt DEAL.

1. Introduction

Circulating fluidized beds (CFBs) operated in fast fluidization regime find wide industrial applications in fluid catalytic cracking and combustion. Further applications include pyrolysis, gasification, and chemical looping technologies. Compared to bubbling and turbulent fluidized beds, CFBs offer a higher heat transfer and contact between gas and solids. Despite many years of research on CFB systems, the flow behavior of single particles and clusters in the riser section is still not fully understood due to complex and fast particle movements, which are difficult to track with most sensors [1]. For model development, optimization of existing processes, and design of new industrial facilities, a better understanding of this topic is of major interest. In CFB systems, particles in the riser are entrained at gas velocities above the single particle terminal velocity. Recirculation of particles is achieved via a cyclone and then reintroduced into the bed (e.g., via loop seals). In the bottom zone of the riser solids volume fractions are highest, which then decrease at higher locations. At higher locations, the dilute zone or fully developed region is defined by low solids concentrations, which remain nearly constant over height (constant pressure gradient $\Delta p/\Delta z$). Solids concentrations in the exit region either increase or remain constant depending on riser dimensions and exit geometry [2,3]. Radially, solids volume fractions show a core-annulus profile, with lean upward particle flow in the center (core) and dense downward flow in the wall region (annulus) at superficial gas velocities up to around 10 m/s. The annulus thickness is roughly one-tenth of the riser diameter. In the core zone, particle clusters with sizes up to several riser diameters can form [4].

In CFBs, common measurement techniques for hydrodynamics include pressure sensors [5], capacitance probes [6,7], and fiberoptic probes [8–11]. For local solids flux and particle velocity measurements, solid extraction probes [12–14] and radioactive particle tracking [15] have been used. Other works combine established methods such as laser Doppler anemometry (LDA) and fiberoptic probes [16]. Complex methods such as positron emission particle tracking (PEPT) [17], electrical capacitance volume tomography [18–20], magnetic resonance imaging (MRI), or X-ray tomography can provide three-dimensional images of a fluidized bed. However, these costly systems cannot be applied to all particle types. Furthermore, the limited time and spatial resolution of these methods can make measurements in CFBs difficult [21]. High-speed imaging is widely used for analyzing single particle movements and clustering in CFBs. Often, rectangular pseudo-2D facilities with very large width-to-depth ratios are used to facilitate imaging [22–27]. However, this increases the friction effect of the wall region on the solids flux. Therefore, only limited conclusions can be drawn about the three-dimensional flow of particles and clusters. Information about the fluidization behavior at the wall region is usually the primary outcome of these measurements.

Borescopic high-speed imaging enables the observation of single particle flows inside fluidized beds. Borescopic particle image velocimetry (PIV) has been used and compared to PEPT in bubbling fluidized beds [28]. Other groups applied borescopic PIV on spouted beds [29,30] and turbulent fluidized beds [31]. For a CFB pilot-scale unit (h_{riser} = 15.6 m, $d_{i,riser}$ = 0.4 m, h_{port} = 6.4 m) Lackermeier et al. [32] first applied borescopic PIV in 2001 in combination with a borescopic laser light sheet technique to visualize two-dimensional flow structures of quartz sand (mean diameter, MD = 192 μm) in the fully developed region. A comprehensive work on PIV in CFBs was published by Shaffer et al. in 2013 [4]. High-speed measurements were conducted with a borescope for internal particle flow and from outside in two pilot-scale CFBs with FCC particles (MD = 70 μm) at Particulate Solid Research, Inc. (h_{riser} = 22 m, $d_{i,riser}$ = 0.2 m, h_{port} = 18 m, superficial gas velocities: 5.8 to 7.6 m/s, solids fluxes: 5 to 30 kg/(m^{2}s)) and with high density polyethylene (HDPE) (MD = 750 μm) at National Energy Technology Laboratory (h_{riser} = 15.5 m, $d_{i,riser}$ = 0.305 m, h_{port} = 9.5 m, superficial gas velocities: 9.1 and 18.3 m/s, solids fluxes: 20 to 400 kg/(m^{2}s)). In these units, one or more jets of high-speed gas could be observed at any time. These jets move from one radial position to another. After moving away, the resulting voids were filled with large clusters of particles with heights up to several riser diameters. Borescopic radial particle velocity measurements showed very high velocities in the center and downward movements (negative velocities) at the riser wall. The core-annulus concentration profile was not observable in real time but emerged by averaging the velocities and concentrations over a significantly longer time periods.

In published literature, there is a scarcity of comprehensive validated data on particle hydrodynamics in CFB risers, especially concerning radial effects. This experimental work aims to fill this gap. The focus is on the flow behavior of FCC catalyst in the fully developed flow region of a pilot-scale CFB riser. From center to wall, two-dimensional particle trajectories were tracked using borescopic high-speed imaging with backlighting and evaluated with particle tracking velocimetry (PTV). The findings are compared to pressure measurements and radial concentration profiles measured with capacitance probes. This work aims to generate new insights into single particle movements on the one hand and to further improve the methodology of imaging techniques for investigating hydrodynamics on the other. The results should contribute to a better understanding of the dynamic interactions within such systems, forming the basis for the development of CFD-DEM models to increase efficiency and scale up processes in industrial applications in the future.

2. Experimental

2.1. Circulating fluidized bed

Fig. 1 shows the CFB setup of the pilot-scale fluidized bed (h_{riser} = 8 m, $d_{i,riser}$ = 0.1 m). Particle circulation is enabled by a loop seal, which connects the standpipe and the riser bottom. The fluidization airflow in the riser is provided by a blower to achieve high gas velocities. The gas enters the riser via a PMMA bubble-cap distributor (4-hole interior riser

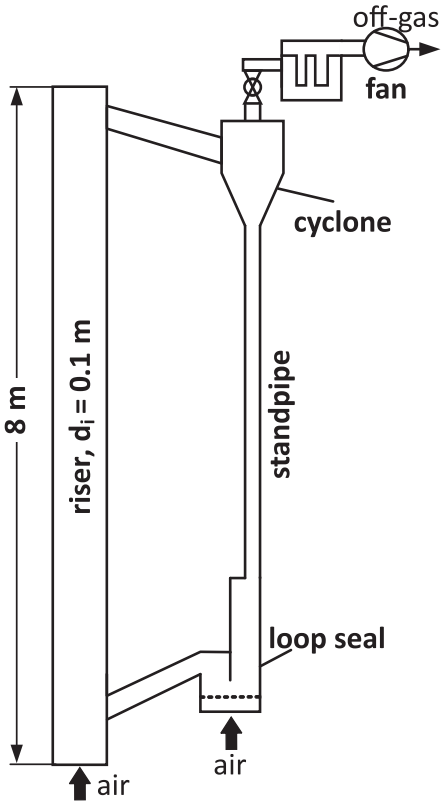


Fig. 1. Scheme of pilot-scale CFB unit at TUHH.

for gas entry with $\phi = 12$ mm holes located 12 mm from the cap). At a height of $h_{port} = 7.06$ m, both capacitance probes and the borescope of the high-speed camera can be inserted to measure solids concentration and particle velocity at different radial positions. Both the upper and lower riser sections (1 m each) as well as the loop seal are made of Poly (methyl methacrylate) (PMMA), allowing visual observation of flow conditions. Other parts of the system are made of steel. The loop seal gas flow is supplied by pressurized air injected via eight PMMA bubble-cap distributors. Dimensions and analysis of gas distribution are found in a prior publication [33].

2.2. Capacitance measurement

Capacitance probes were used to determine local solids concentrations. A major advantage of this technique is its applicability to measurements at high solids concentration (e.g. bubbling fluidized bed, BFB) and in dilute flows (e.g. CFB). The basic operating principle of a capacitance probe is the change in dielectric constant in the electric field between two electrodes. This change relates to the solids concentration. Various approaches exist in the literature to calculate solids concentration from the changing dielectric constant. For this work, the following linear relation published by Wiesendorf and Werther [6] for gas-solid systems under ambient conditions is used:

$$c_v = c_{v,fb}\frac{(K_e - K_{e,f})}{\left(K_{e,fb} - K_{e,f}\left(1 + \frac{(K_{e,fb}-K_e)(K_{e,fb}-3)}{K_{e,fb}\cdot K_{e,f}}\right)\right)} \quad (1)$$

$$K_e = \frac{U_f}{U_e} \quad (2)$$

c_v is the solids concentration, $c_{v,fb}$ is the solids concentration of the fixed bed, K_e is the dielectric constant of the suspension, $K_{e,fb}$ is the dielectric constant at fixed bed concentration, and $K_{e,f}$ is the dielectric constant of the fluid. The dielectric constants are calculated from the voltage of air U_f divided by the voltage signal of the fixed bed $U_{e,fb}$ or suspension U_e. Fig. 2 shows a schematic of the two-channel capacitance probe used. Both channels consist of three electrodes: a tungsten core electrode, ground electrode, and guard electrode between the channels. The guard electrode shields the core from electric fields to enable formation of a constant electric field, which is required for accurate measurements. The distance between the two channels d_{ch} is 4 mm with an electrode length of 3 mm. The probe diameter d_{cap} is 8 mm. For this work, only one probe channel was used.

2.3. Borescopic high-speed camera system

For high-speed imaging a high-speed camera (model IDT NX4-S2 by Integrated Design Tools, Inc.) connected to a borescope (length = 60 cm, diameter = 1 cm) was used to record and track particles in the circulating fluidized bed. Fig. 3 shows the camera, connected to the borescope and PMMA riser section. For illustration, two frames captured by the camera are shown. Due to the background light, particles appear dark on the white background.

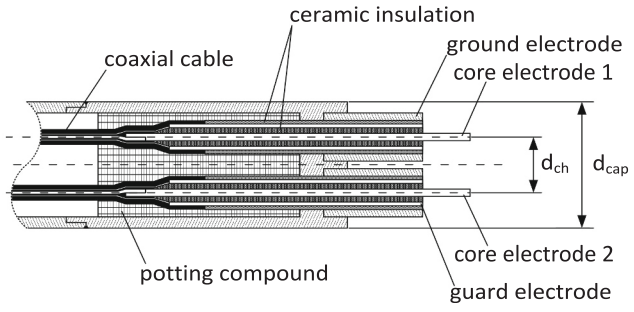


Fig. 2. Schematic of capacitance probe used in this work [7].

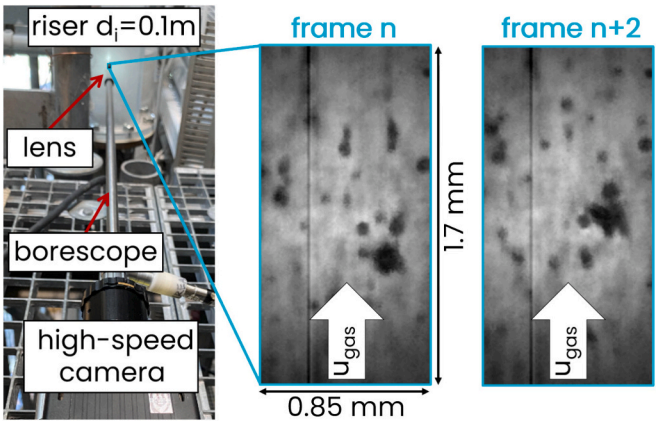


Fig. 3. Left: IDT NX4-S2 high-speed camera connected to borescope (60 cm length) and riser. **Right:** Two video frames at 15,600 fps with visible single particles.

Fig. 4 shows a sketch of the setup with camera, borescope and connecting tube with LED. An opening in the connecting tube enables upward and downward particle flow through the measurement region between borescope lens and LED (LED-lens distance = 2 mm). The connecting tube has a diameter of 12 mm. All measurement conditions are listed in the experimental overview.

2.4. Particle tracking velocimetry

While PIV is based on the Eulerian measurement principle (velocity as a function of position and time), PTV is based on the Lagrangian measurement principle. PTV tracks individual particle trajectories in successive images, which is particularly suitable for flows with low particle concentrations [34]. Advanced algorithms, e.g., those using velocity gradient tensors or multi-frame tracking, have been developed to improve accuracy, especially in complex flows [12]. PTV can offer higher spatial resolution but is more computationally intensive than PIV.

For this work, a code written in MATLAB (R2025b) was used to determine the velocity of individual particles in a video by tracking their centroid across frames. Particles are detected via gray scales. Due to the background light, they appear dark on the white background. The images were binarized using local adaptive thresholding (function: *imbinarize*) with a sensitivity factor of 0.45. Local adaptive thresholding was chosen because the LED emission profile and the borescope optics produce a brighter central region that falls off toward the edges of the frame. The method determines the threshold from the neighborhood of each pixel and adapts frame by frame to the spatially non-uniform brightness. The matching of centroids of the same particle across frames was done using James Munkres's variant of the Hungarian assignment algorithm [35] (function: *assignDetectionsToTracks*), where the assignment cost is defined as the deviation of the inter-frame displacement from a reference particle velocity. The reference velocity is set to 60% of the superficial gas velocity of the respective operating condition. It serves to rank candidate matches that have already satisfied the constraints described below and does not by itself determine which matches are admissible. Each track is followed across frames by recording how many frames it has existed and whether a detection could be matched to it in the current frame. A track is terminated once a frame passes without a match. Due to particle collisions and overlapping trajectories, a set of input parameters was defined to ensure the evaluation of realistic and consistent particle trajectories. Only tracks visible for at least five frames were included. Since a particle must therefore remain within the field of view for at least five frame intervals, this criterion

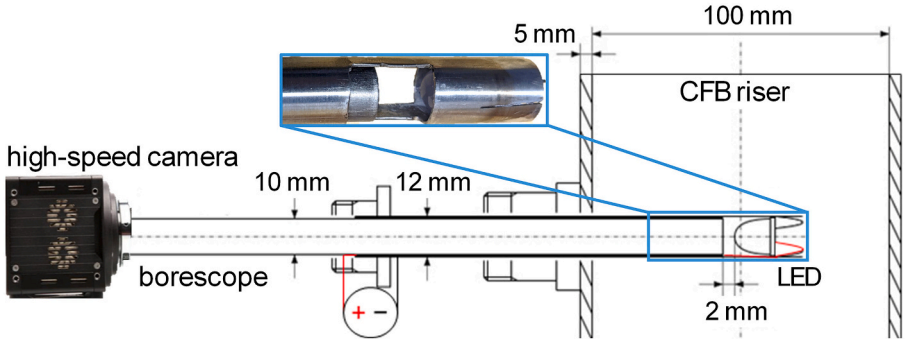


Fig. 4. Sketch of setup for borescopic high-speed imaging connected to CFB riser.

imposes an upper limit on the measurable particle velocity, given by the field of view along the direction of motion divided by the duration of five frame intervals. Since the flow in the riser is predominantly axial, a particle is expected to move approximately parallel to the riser axis between two consecutive frames, and trajectories with horizontal jumps larger than 10 pixels per frame were therefore excluded at the used resolution of 256 × 128 pixels (height × width). Furthermore, minimum and maximum particle velocities were defined to exclude particles stuck at the lens and overestimations of particle velocities. In the core zone (radial position 0–3 cm), only upward moving trajectories were evaluated. Closer to the wall (radial position 4 and 5 cm), velocities in both upward and downward directions were evaluated.

2.5. Solids flux

The solids flux, G_s in the CFB unit was determined by quickly interrupting the fluidization in the loop seal for five to ten seconds and measuring the height of the solids accumulated in the standpipe. Using the bulk density, G_s is then calculated. Each measurement was conducted at least five times.

Local solids flux

In CFB risers, the flow is characterized by changing velocity profiles and inhomogeneous solids distributions. A local (radial) analysis can deliver a deeper understanding of particle movement and identify zones with high or low particle movement. The local solids flux $G_{s,local}$ is calculated from measured radial solids volumetric concentrations c_v (from capacitance probes) and corresponding local particle velocities u_p (from borescopic PTV), both available in this study. For particles moving with a velocity u_p and a solids concentration c_v at one radial position, the local solids flow per cross section q_s ($m^3_{solids}/m^2_{cross\text{-}section} \cdot s = m/s$) is:

$$\boldsymbol{q_s} = \boldsymbol{c_v} \cdot \boldsymbol{u_p} \tag{3}$$

Assuming homogeneous particle properties and known bulk density ρ_{bulk}, the local solids flux at each radial position is:

$$\boldsymbol{G_{s,local}} = \boldsymbol{q_s} \cdot \boldsymbol{\rho_{bulk}} = \boldsymbol{c_v} \cdot \boldsymbol{u_p} \cdot \boldsymbol{\rho_{bulk}} \tag{4}$$

A radial average of local solids fluxes from center to wall should equal the overall solids flux, can be compared to directly measured solids flux values as a validation step. Since c_v and u_p are obtained from two independent measurements, the local solids flux is calculated from their time-averaged values at each radial position. Correlations between the instantaneous fluctuations of solids concentration and particle velocity are therefore not captured.

2.6. Experimental overview

In the fast fluidization regime, the hydrodynamic behavior of FCC catalyst (Sauter mean diameter = 61.5 μm) was investigated in the fully developed region of a CFB riser for four superficial gas velocities ($u_{g,riser}$ = 2, 3, 4, and 5 m/s). Capacitance probes and borescopic high-speed imaging were used for radial solids concentration measurement and particle velocimetry. Initial tests with higher solids fluxes, controlled by higher loop seal fluidization velocities, led to too high solids concentrations in the fully developed region, preventing tracking of individual particles in the wall region. Table 1 lists the process conditions used, better suited for single particle tracking in both core and annular regions. After initial tests with LED-lens distance of 4 mm, the distance was reduced to 2 mm to increase light intensity and minimize the influence of different particle flow layers in the background. The solids inventory in the system was 13.7 kg.

For every operation point, measurements were conducted from the wall (rad. pos. = 5 cm, sensor depth = 0 cm) to the center (rad. pos. = 0 cm, sensor depth = 5 cm). Due to the invasive nature of the sensors, only half profiles were measured to minimize their influence on particle flow. Radial symmetry was assumed in the fully developed flow region. Solids concentrations were measured with capacitance probes (60 s at 1000 Hz). Videos were recorded with the borescopic high-speed camera system at a resolution of 256 × 128 pixels (height × width), corresponding to 1.70 mm × 0.85 mm at 1 mm focus distance from the lens. Particles at larger distances from the lens appear smaller and increasingly out of focus, and are largely rejected during binarization, so that only particles within a limited depth around the focal plane are evaluated. The frame rate was 15,600 fps with 50 μs exposure time, sensor gain of 1 and 8-bit (low) pixel depth. With the frame rate and field of view used, the requirement of tracking a particle for at least five frames corresponds to an upper limit of approximately 5.3 m/s for the measurable particle velocity. The displacement of a particle during the used exposure time leads to image blur. Since this blur is symmetric with respect to the particle position at the midpoint of the exposure, it does not displace the centroid and therefore does not bias the measured velocity. It does, however, reduce the contrast of fast-moving particles, so that the detection becomes less reliable with increasing particle velocity. For each condition, 100 videos of 1000 frames each, were recorded and evaluated. The time between each measurement was at least 5 s to ensure better representation of steady state.

3. Results and discussion

3.1. PTV sensitivity analysis

The developed PTV script was validated via synthetic *MATLAB*-generated video data mimicking experimental resolution and frames

Table 1
Operating conditions used for this work.

$u_{g,riser}$ (m/s)	G_s (kg/m^{2}s)	$u_{g,loop\ seal}$ (m/s)
2	3.1	0.024
3	8.0	
4	14.9	
5	19.3	

(256 × 128 pixels, 1000 frames). 100 to 40,000 upward moving particles per 1000 frames were generated randomly, starting from the bottom of each frame. The goal of this is to emulate varying solids concentrations. Particle velocities were set to values evenly spaced at 1.2, 1.4, 1.8, or 2.0 m/s, with an average velocity of 1.6 m/s. An example frame of a measurement and three frames from synthetic videos with different solids concentrations are shown in Fig. 5.

Fig. 6 shows the number of tracked particles by the PTV script versus generated particles per 1000 frames. For lower numbers of generated particles, all particles were tracked (proportional factor = 1, see black line) and velocities were correctly evaluated. Above approx. 2000 particles, tracking ability declines due to trajectory overlaps, worsening with increased solids concentration. For more than 8000 particles per 1000 frames, the number of particles captured decreases with increasing solids concentration. At these conditions, the average detected particle velocity is around 0.1 m/s below the actual average velocity of 1.6 m/s. Despite limitations at higher solids, the method reasonably represents actual conditions. Excessively high solids concentrations should be avoided for reliable single particle tracking. Beyond the overall solids concentration, the flow structure introduces a systematic effect. Particle clusters represent regions of locally increased solids concentration, and since the field of view covers only a small volume, the particle number within a cluster corresponds locally to the upper range of Fig. 6. Particles within clusters are therefore less likely to be tracked than particles in the more dilute regions between them.

3.2. Solids concentration profiles

Fig. 7 (a) shows radial solids concentration profiles measured with capacitance probes for FCC catalyst at superficial gas velocities of $u_g = 2$, 3, 4, and 5 m/s and the corresponding solids fluxes. Radial position 0 cm corresponds to riser center, 5 cm to the wall. To better visualize the trends, lines are added to the plot. A core-annular flow profile is observed in all cases with sharp concentration increases starting about 2 cm from the wall. Standard deviations increase toward the wall. While the particle flow in the core zone can be seen as homogeneous upward flow, at the wall there occurred either voids or particle cluster flow alternating between upward and downward movement, which was observable at the PMMA sections. These observations confirm prior findings of high-speed gas jets and large clusters of particles, which fill the voids in the riser wall region [4]. Comparable radial solids concentration profiles were measured by Pugsley et al. [36] using electrical capacitance tomography (ECT) and fiber optic probes with FCC catalyst (Sauter mean diameter = 89 μm, $u_{mf} = 0.57$ cm/s) in a similar sized CFB riser ($d_{i,riser} = 0.14$ m, $h = 7$ m) at $u_g = 4.7$ m/s with higher solids fluxes

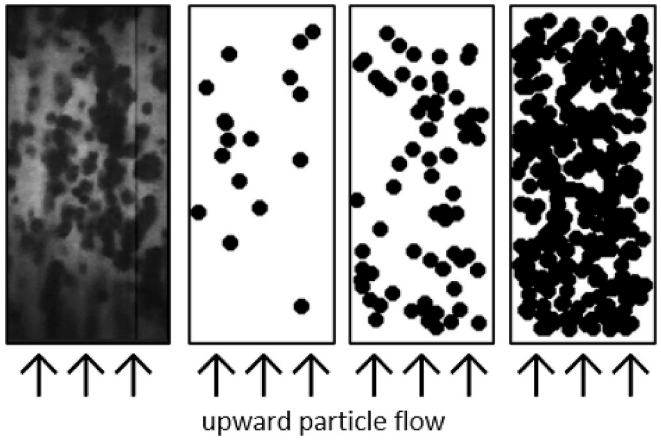


Fig. 5. Left: Single imaging frame (rad. pos. = 0 cm, $u_g = 4$ m/s). Right: Single frames of synthetic data with 1000, 4000 and 20,000 particles generated per 1000 frames.

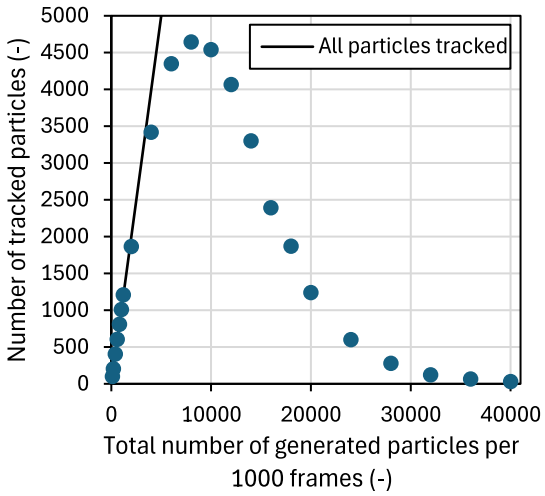


Fig. 6. Tracks detected versus particles generated per 1000 frames.

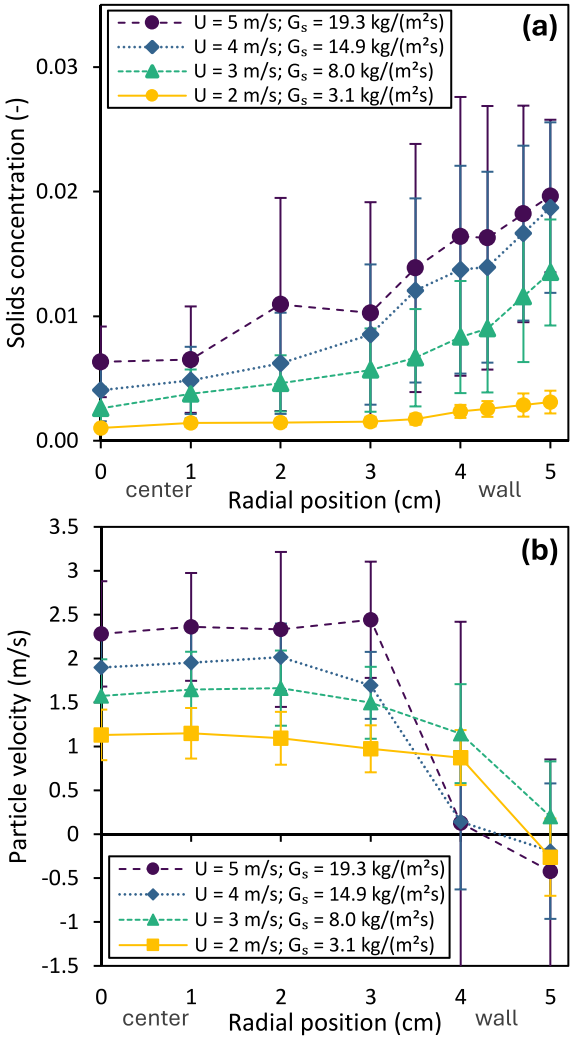


Fig. 7. Radial profiles of solids concentration (a) and particle velocity (b) of FCC catalyst in CFB riser captured with capacitance probes and borescopic high-speed imaging at 7.06 m port height. (U = u_g).

of 148 and 263 kg/(m^{2}s). The measured solids concentrations at $u_g = 2$ m/s are significantly lower and the profile is flatter with less differences

between core and wall region. This is likely caused by lower solids flux, which leads to a lower accumulation of particles in the wall region.

3.3. Particle velocity profiles

Fig. 7 (b) shows radial particle velocities of the FCC catalyst in the CFB riser measured via borescopic high-speed PTV (100,000 frames per measurement point). Again, the results match a core-annular flow. In the core zone (rad. pos. 0–3 cm) constant high particle velocities were detected. At the wall, mostly negative particles velocities were observed. Only for a superficial gas velocity of 3 m/s the velocities at the wall were mostly positive. This can be led back to a transition or built-up of higher solids concentrations in the annular zone. At 2 m/s the lowest upward forces are exerted on the particles. With low solids concentrations, no significant annulus is built up in the wall region. Therefore, negative particle velocities are caused by wall friction. At superficial gas velocities 4 and 5 m/s solids concentrations at the wall region are highest and particle velocities are much closer to the ones at the wall. This indicates an increase in the annular thickness with higher superficial gas velocities and solids fluxes, which was also described by Weber et al. [37]. With higher solids volume fraction in the annulus, more downward moving particle clusters exert friction against the upward core flow. Table 2 summarizes the evaluated particle trajectories per measurement. In the wall region (rad. pos. 4 and 5 cm) velocities in both upward and downward direction were evaluated. Due to high solids concentration in the wall zone, images are darker and tracking of single particle trajectories becomes more difficult. This is seen in the low number of particle trajectories in the wall region for all measurements. At $u_g = 5$ m/s a lower quantity of trajectories was detected in the riser center. This is likely caused by the relatively high exposure time of 50 µs, leading to images with lower sharpness. In the case that every particle was tracked, the number of detected particles could be used for a validation solids concentration profiles. However, due to the limitations of PTV and the setup in this work, this was not possible.

For example, Fig. 8 shows the number and velocity distribution of particles, tracked at for a 1000 frame video at $u_g = 2$ m/s ($G_s = 3.1$ kg/(m^{2}s)) (left) and 5 m/s ($G_s = 19.3$ kg/(m^{2}s)) (right) at the riser center. With higher gas velocities and solids fluxes, the distribution of measured particle velocity gets broader. This explains the higher standard deviations at higher gas velocities in the radial particle velocity measurements. In accordance with the solids concentration profiles, the standard deviations also increase with positions closer to the wall. This is most distinctive for higher gas velocities and higher solids fluxes, where more particles are present in the wall region.

A comparison between solids concentration and particle velocity in the core flow zone (0–3 cm rad. pos.) is presented in Fig. 9. Average solids concentrations are based on the annulus area around the probe tip with the assumption of radial symmetry in the riser. Measurement positions closer to the wall represent larger areas in the riser. For both $c_{v,core}$ and $u_{p,core}$ almost linear increases with superficial gas velocity are observed (see Table 3). Larger standard deviations occur at higher velocities due to cluster and void formation and complex radial interactions caused by annulus buildup.

For all operating conditions used, the ratio of $u_{p,core}/u_g$ was close to 0.5. In literature $u_{p,core}/u_g$ ratios above 1 were reported for quartz sand [9] and FCC [10,11]. The measurements in these works were conducted with much higher solids fluxes. With this, more particles accumulate in the wall region which leads to higher gas velocities and therefore higher particle velocities in the core flow zone [10]. Thus, higher $u_{p,core}/u_g$ ratios can be achieved with increasing solids flux while keeping constant

Table 2
Number of evaluated particle trajectories.

rad. pos. (cm)	2 m/s	3 m/s	4 m/s	5 m/s
5 (wall)	31,770	20,067	8184	8837
4	50,388	32,189	12,495	40,206
3	58,017	53,444	10,274	29,240
2	43,194	40,853	45,632	24,422
1	18,044	41,454	43,470	17,936
0 (center)	14,660	47,552	35,405	17,685

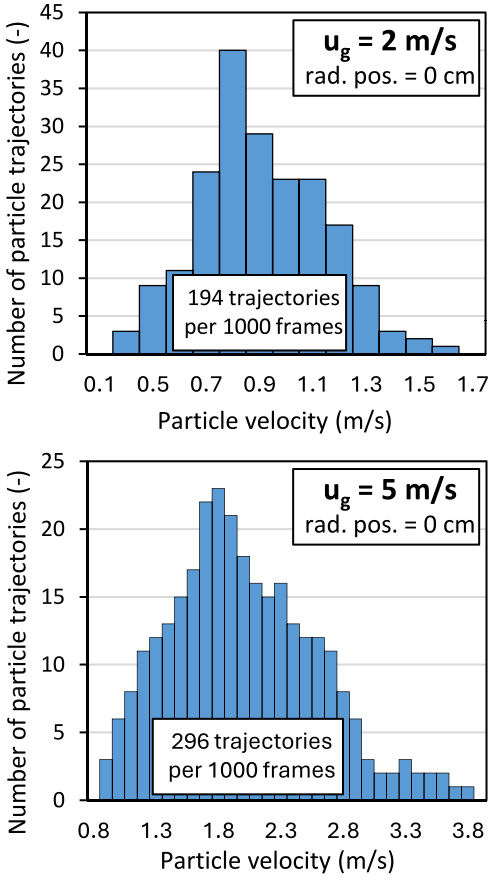


Fig. 8. Example particle velocity distribution from one video (1000 frames, 15,600 fps) at the radial riser center (rad. pos. = 0 cm, center) for superficial gas velocities of 2 and 5 m/s.

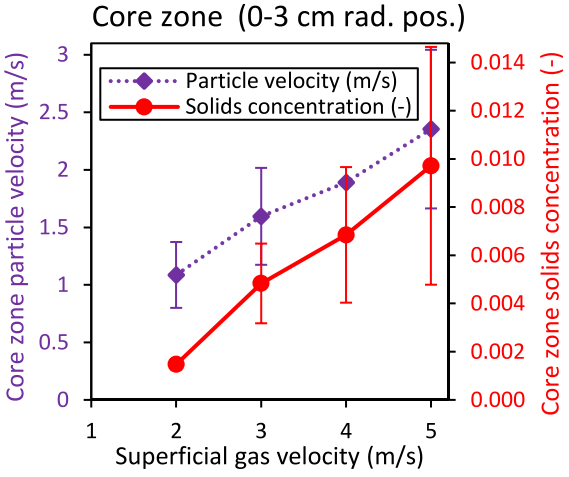


Fig. 9. Average solids concentration and particle velocity in core zone (0–3 cm rad. pos.) of FCC catalyst in CFB riser captured with capacitance probes and borescopic high-speed imaging at 7.06 m port height. The corresponding solids flux values are shown in Table 1.

Table 3
Particle velocity and solids concentration in core zone.

u_g (m/s)	$u_{p,core}$ (m/s)	$u_{p,core}/u_g$	$c_{v,core}$
2	1.09	0.55	0.0015
3	1.60	0.53	0.0048
4	1.89	0.47	0.0068
5	2.35	0.47	0.0097

gas velocity. Schaffer et al. [4] confirmed this trend at high u_g (18.3 m/s) but observed the opposite at lower u_g (9.15 m/s). Thus, no general prediction of particle velocities in the core flow zone can be made yet. This emphasizes the importance of validated comprehensive experimental data sets.

3.4. Comparison of measurement techniques

Fig. 10 compares average solids concentrations of the FCC catalyst from capacitance probes together with solids concentrations from pressure measurements and gray values from borescopic high-speed imaging. Pressure differences were measured 20 cm below and above probe port. A gray value of 0% corresponds to a white video (only background light without any particles) and 100% to an almost black video, where the background light is completely blocked by particles. From this, the raw imaging data can be used to estimate the solids concentration trends. All three trends show a comparable development of higher values with higher superficial gas velocities. While the solids concentration from capacitance probes increases almost linearly, the trends from pressure measurement flatten with higher superficial gas velocities. This flattening is unlikely since all radial c_v from capacitance measurements (Fig. 7, (a)) are highest for $u_g = 5$ m/s. By considering the low solids concentrations around 0.01 or 1 vol% and high standard deviations at higher gas velocities, these trends can still be considered as cross-validation of the three different measurement techniques used.

3.5. Solids flux analysis

As introduced in Section 2.5, the local solids flux describes the solids circulation in upward direction for a radial position of riser. It depends on solids concentration, particle velocity and solids density. Fig. 11 shows local solids fluxes versus radial position. With higher superficial gas velocities and solids fluxes, a clear increase in the local solids flux can be seen. The shape of the profiles is characterized by increases in the rate from the center of the system up to the radial position 3 cm. This is caused by constant particle velocities in core zone, while solids concentration increased steadily with positions closer to the wall. Due to the partially negative particle velocities at the two radial positions 4 and 5 cm, the local solids flux decreases in the wall region. In the core zone, the standard deviations are in a range of 0.5 up to 1 of the local solids flux values. The high values result from the sum of standard deviations of the particle velocities and solid concentrations. In the wall region, standard deviations are up to 15 times higher than the average local solids flux. This is partly due to the mentioned dependency of two measurement types, but mainly because of both the upward and downward particle flow in the wall region. For clarity, these are not shown in the plot.

From the profiles of the local solids fluxes, an average solids flux can be calculated across the cross-section of the riser. Fig. 12 shows the averaged local solids flux, compared to global solids flux, which was measured independently. Table 4 lists global and averaged local solids fluxes with their respective standard deviations. Both solids flux measurements show a similar trend and are of a similar magnitude. The deviations between the averaged local solids flux and the measured solids flux result from inaccuracies of the measurement methods. Electrostatic charge and the limitations of single particle tracking are the main causes of these fluctuations. The highest deviations are seen at u_g = 4 m/s and 5 m/s which potentially indicates that the fastest particles

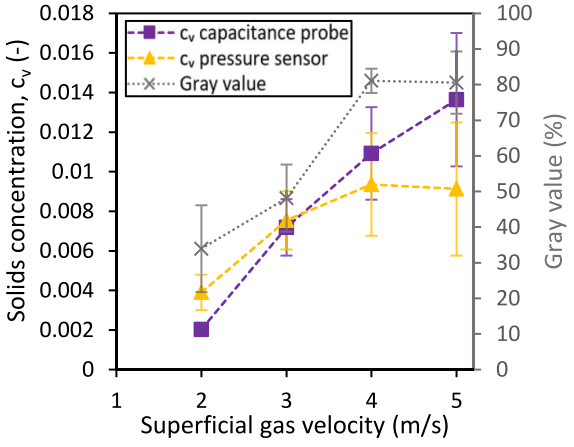


Fig. 10. Comparison of average solids concentration of FCC catalyst for 2–5 m/s superficial gas velocity in fully developed riser region (7.06 m port height) calculated from data of capacitance probe, pressure measurement and high-speed imaging (gray values). The corresponding solids flux values are shown in Table 1.

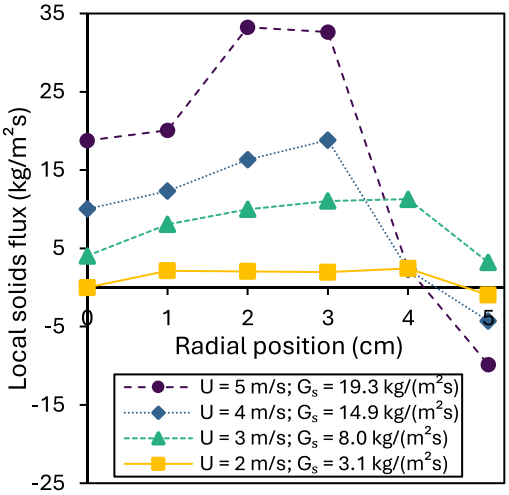


Fig. 11. Radial trend of solids flux for FCC catalyst against superficial gas velocities and solids fluxes in the riser.

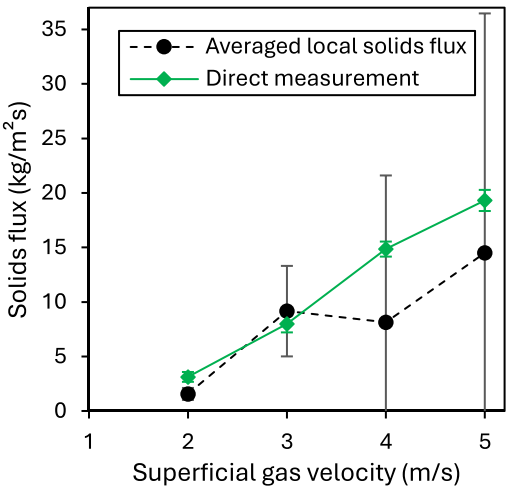


Fig. 12. Averaged local versus measured solids flux comparison.

Table 4
Averaged local and measured solids flux values.

u_g (m/s)	$G_{s,direct}$ (kg/m^2/s)	Std.dev.$G_{s,direct}$ (kg/m^2/s)	$G_{s,local}$ (kg/m^2/s)	Std.dev.$G_{s,local}$ (kg/m^2/s)
2	3.13	0.45	1.48	0.55
3	7.90	0.77	8.71	4.15
4	14.85	0.69	7.39	13.47
5	19.31	0.97	14.50	21.72

were under-represented in the PTV measurements. This is likely caused by the lower contrast of fast-moving particles in the video data. Even with the measurement limitations, this comparison serves as a further validation for the measurement techniques used.

4. Conclusion

This study investigated FCC catalyst hydrodynamics in a pilot-scale CFB riser at four gas velocities. For the first time, direct comparisons of radial profiles of solids concentration via capacitance probes and particle velocities via borescopic high-speed imaging were conducted. In all operating conditions, a core-annular flow was observed, with low solids concentrations in the center and higher ones in the wall region. Borescopic high-speed PTV provided radial single-particle velocity data in upward and downward directions. In the core zone, particle velocities increased linearly with gas velocity at $u_{p,core}/u_g$ of roughly 0.5 for a solids flux range of 3 to 20 kg/(m^{2}s). Based on the radial data of solids concentrations and particle velocities, local solids fluxes were determined. Averages of these trends mostly agreed with trends of directly measured solids fluxes. PTV was demonstrated as reliable tool at low solids concentrations but limited at higher solids concentrations due to particle trajectory overlaps. This work provides fundamental validated data on single particle flow in a CFB riser useful for CFD-DEM model validation.

CRediT authorship contribution statement

Lennard Lindmüller: Writing – review & editing, Writing – original draft, Visualization, Validation, Methodology, Investigation, Formal analysis, Data curation, Conceptualization. **Stefan Heinrich:** Writing – review & editing, Supervision, Funding acquisition. **Benjamin Rahimian:** Software. **Jörg Theuerkauf:** Supervision. **Yuan Yao:** Project administration. **Yi Fan:** Supervision.

Declaration of competing interest

The authors declare the following financial interests/personal relationships which may be considered as potential competing interests: Lennard Lindmueller reports financial support, administrative support, and equipment, drugs, or supplies were provided by The Dow Chemical Company. If there are other authors, they declare that they have no known competing financial interests or personal relationships that could have appeared to influence the work reported in this paper.

Acknowledgments

This work was funded by The Dow Chemical Company, United States under award no. 223278AW.

Data availability

Data will be made available on request.

References

[1] J. Grace, X. Bi, N. Ellis (Eds.), Essentials of Fluidization Technology, Wiley, 2020.
[2] U. Lackermeier, J. Werther, Flow phenomena in the exit zone of a circulating fluidized bed, Chem. Eng. Process. Process Intensif. 41 (2002) 771–783.
[3] X.-B. Qi, J. Zhu, W.-X. Huang, A new correlation for predicting solids concentration in the fully developed zone of circulating fluidized bed risers, Powder Technol. 188 (2008) 64–72.
[4] F. Shaffer, B. Gopalan, R.W. Breault, R. Cocco, S.R. Karri, R. Hays, T. Knowlton, High speed imaging of particle flow fields in CFB risers, Powder Technol. 242 (2013) 86–99.
[5] J. Werther, Measurement techniques in fluidized beds, Powder Technol. 102 (1999) 15–36.
[6] V. Wiesendorf, J. Werther, Capacitance probes for solids volume concentration and velocity measurements in industrial fluidized bed reactors, Powder Technol. 110 (2000) 143–157.
[7] T. Wytrwat, E.-U. Hartge, M. Yazdanpanah, S. Heinrich, Influences on the transition from bubbling to turbulent fluidization for Geldart's group B particles, Powder Technol. 375 (2020) 81–88.
[8] P. Schlichthaerle, J. Werther, Axial pressure profiles and solids concentration distributions in the CFB bottom zone, Chem. Eng. Sci. 54 (1999) 5485–5493.
[9] J. Zhou, J.R. Grace, C.J. Lim, C. Brereton, Particle velocity profiles in a circulating fluidized bed riser of square cross-section, Chem. Eng. Sci. 50 (1995) 237–244.
[10] J. Pärssinen, J.-X. Zhu, Particle velocity and flow development in a long and high-flux circulating fluidized bed riser, Chem. Eng. Sci. 56 (2001) 5295–5303.
[11] Y. Fan, C. Li, H. Fan, M. Yu, C. Lu, Core-Annulus radial solids concentration distribution in riser, Chem. Eng. Sci. 192 (2018) 318–334.
[12] M. Ishikawa, Y. Murai, A. Wada, M. Iguchi, K. Okamoto, F. Yamamoto, A novel algorithm for particle tracking velocimetry using the velocity gradient tensor, Exp. Fluids 29 (2000) 519–531.
[13] T. Wytrwat, Fluid Dynamics of Turbulent Fluidized Beds for Geldart's Group B Particles, Doctoral dissertation, Hamburg University of Technology, Cuvillier Verlag, Göttingen, 2022.
[14] A.S. Issangya, S.B.R. Karri, R.A. Cocco, T. Knowlton, J.W. Chew, Solids flux profiles of Geldart Group A particles in high-velocity circulating fluidized bed risers, Can. J. Chem. Eng. 101 (2023) 256–268.
[15] T. Tribedi, P. Pillajetti, R. Kumari, H.J. Pant, P. Tiwari, R.K. Upadhyay, Measurements of solid velocity in a pilot-scale Geldart's Group B circulating fluidized bed using a radioactive particle tracking technique, Ind. Eng. Chem. Res. 61 (2022) 9110–9121.
[16] J. Werther, B. Hage, C. Rudnick, A comparison of laser Doppler and single-fibre reflection probes for the measurement of the velocity of solids in a gas-solid circulating fluidized bed, Chem. Eng. Process. Process Intensif. 35 (1996) 381–391.
[17] M. Stein, Y. Ding, J. Seville, D. Parker, Solids motion in bubbling gas fluidised beds, Chem. Eng. Sci. 55 (2000) 5291–5300.
[18] W. Warsito, Q. Marashdeh, L.-S. Fan, Electrical capacitance volume tomography, IEEE Sensors J. 7 (2007) 525–535.
[19] B. Watson, L. Lindmüller, S. Heinrich, J. Theuerkauf, Y. Yao, Y. Fan, Dynamic bubble tracking in fluidized beds via electrical capacitance volume tomography, Chem. Eng. J. 487 (2024) 150461.
[20] R.W. Breault, J. Weber, L.J. Shadle, The development of a generalized riser flow regime map based upon higher moment and chaotic statistics using electrical capacitance volume tomography (ECVT), Powder Technol. 365 (2020) 12–27.
[21] A. Penn, C.M. Boyce, T. Kovar, T. Tsuji, K.P. Pruessmann, C.R. Müller, Real-time magnetic resonance imaging of bubble behavior and particle velocity in fluidized beds, Ind. Eng. Chem. Res. 57 (2018) 9674–9682.
[22] C. Wang, Z. Li, J. Wei, X. Lan, M. Ye, J. Gao, Quantitative measurement of solids holdup for Group A and B particles using images and its application in fluidized bed reactors, Processes 10 (2022) 610.
[23] X. Wei, J. Zhu, Experimental investigation of the instantaneous flow structure in circulating fluidized bed: phase characterization and validation, Chem. Eng. Sci. 228 (2020) 115946.
[24] D. Xiao, X. Dong, S. Hu, X. Liu, Coupling particle image velocimetry and digital image analysis to characterize cluster dynamics in a fast fluidized bed, Powder Technol. 434 (2024) 119267.
[25] S. Yin, W. Zhong, T. Song, P. Lu, Y. Chen, Clusters identification and meso-scale structures in a circulating fluidized bed based on image processing, Adv. Powder Technol. 30 (2019) 3010–3020.
[26] X. Wei, J. Yang, J. Zhu, Experimental analysis of phase segregation in gas-solid circulating fluidized bed riser with direct image calibration, Chem. Eng. J. 379 (2020) 122301.
[27] A.E. Carlos Varas, E. Peters, J. Kuipers, Experimental study of full field riser hydrodynamics by PIV/DIA coupling, Powder Technol. 313 (2017) 402–416.
[28] M. Banaei, R. Dellaert, N.G. Deen, J. Kuipers, M. van Sint Annaland, Borescopic particle image velocimetry in bubbling gas–solid fluidized beds, Particuology 43 (2019) 66–75.
[29] A. Atxutegi, M. Tellabide, G. Lopez, R. Aguado, J. Bilbao, M. Olazar, Implementation of a borescopic technique in a conical spouted bed for tracking spherical and irregular particles, Chem. Eng. J. 374 (2019) 39–48.
[30] L. Qian, Y. Lu, W. Zhong, B. Jin, Developing a high speed fiber-optic endoscopic technique for measuring particle phase characteristics in a spouted bed, Procedia Eng. 102 (2015) 150–158.
[31] S. Tebianian, K. Dubrawski, N. Ellis, R.A. Cocco, R. Hays, S.R. Karri, T. W. Leadbeater, D.J. Parker, J. Chaouki, R. Jafari, P. Garcia-Trinanes, J.P. Seville, J. R. Grace, Solids flux measurements via alternate techniques in a gas-fluidized bed, Chem. Eng. J. 306 (2016) 306–321.
[32] U. Lackermeier, C. Rudnick, J. Werther, A. Bredebusch, H. Burkhardt, Visualization of flow structures inside a circulating fluidized bed by means of laser sheet and image processing, Powder Technol. 114 (2001) 71–83.

[33] L. Lindmüller, J. Haus, A. Ramesh Kumar Nair, S. Heinrich, Minimizing gas leakages in a system of coupled fluidized bed reactors for chemical looping combustion, Chem. Eng. Sci. 250 (2022) 117366.
[34] F. Sijie, B. Pascal-Henry, M. Christian, A comparative study of particle image velocimetry (PIV) and particle tracking velocimetry (PTV) for airflow measurement, in: ICFDT 2015: 17th International Conference on Fluid Dynamics and Thermodynamics, 2015, 2015.
[35] J. Munkres, Algorithms for the assignment and transportation problems, J. Soc. Ind. Appl. Math. 5 (1957) 32–38.
[36] T. Pugsley, H. Tanfara, S. Malcus, H. Cui, J. Chaouki, C. Winters, Verification of fluidized bed electrical capacitance tomography measurements with a fibre optic probe, Chem. Eng. Sci. 58 (2003) 3923–3934.
[37] J.M. Weber, M.M. Bobek, R.W. Breault, J.S. Mei, L.J. Shadle, Investigation of core-annular flow in an industrial scale circulating fluidized bed riser with electrical capacitance volume tomography (ECVT), Powder Technol. 327 (2018) 524–535.